Supporting information for:

pH Control of Conductance in a Pyrazolyl Langmuir-Blodgett Monolayer

L. Herrer,[a,b] S. Martín,[a,b,c] A. González-Orive,[d] D. C. Milan,[e] A. Vezzoli,[e] R. J. Nichols,[e*] J. L. Serrano,[a,f*] and P. Cea.[a,b,e*]

[a] Instituto de Nanociencia y Materiales de Aragón (INMA), CSIC-Universidad de Zaragoza, Zaragoza 50009, Spain.

[b] Departamento de Química Física, Facultad de Ciencias, Universidad de Zaragoza, 50009, Zaragoza, Spain.

[c] Laboratorio de Microscopias Avanzadas (LMA). Universidad de Zaragoza, Edificio I+D+i. 50018, Zaragoza, Spain.

[d] Department of Chemistry, Materials and Nanotechnology Institute, University of La Laguna, 38200, La Laguna, Tenerife, Canary Islands, Spain.

[e] Department of Chemistry, University of Liverpool, Crown Street, Liverpool, L69 7ZD, United Kingdom.

[f] Departamento de Química Orgánica, Facultad de Ciencias, Universidad de Zaragoza, 50009, Zaragoza, Spain.

Content

1. ^{1}H-NMR, ^{13}C-NMR, UV-Vis.

Figures S1, S2 and S3 show the ^{1}H-NMR, ^{13}C-NMR, and UV-Vis spectra of compound **1** in solution.

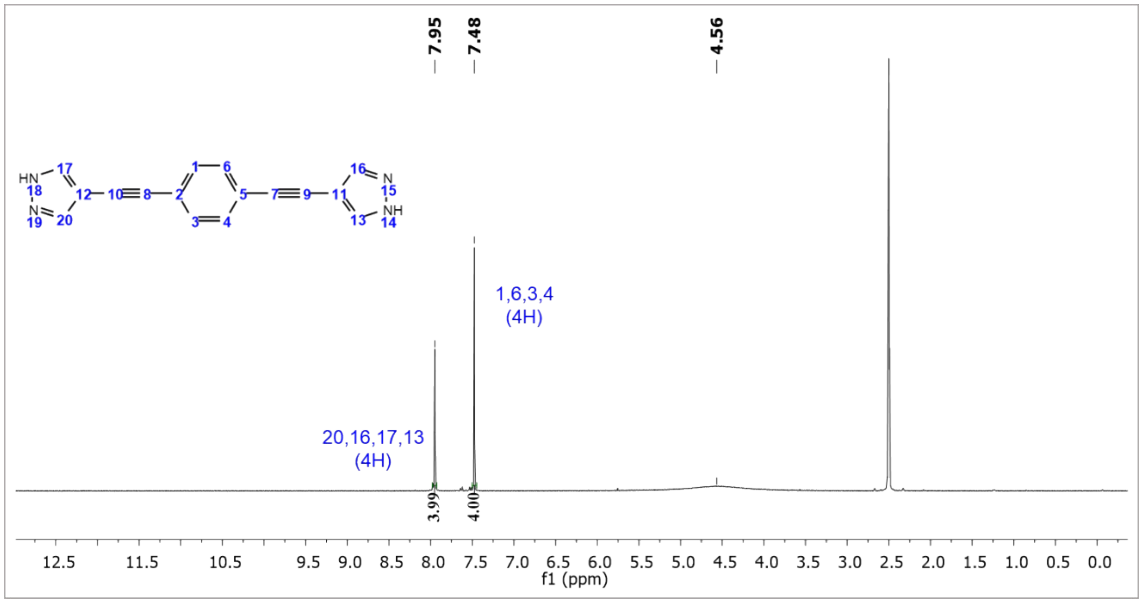

Figure S1. ^{1}H-NMR of compound **1** in DMSO-d6, 400 MHz.

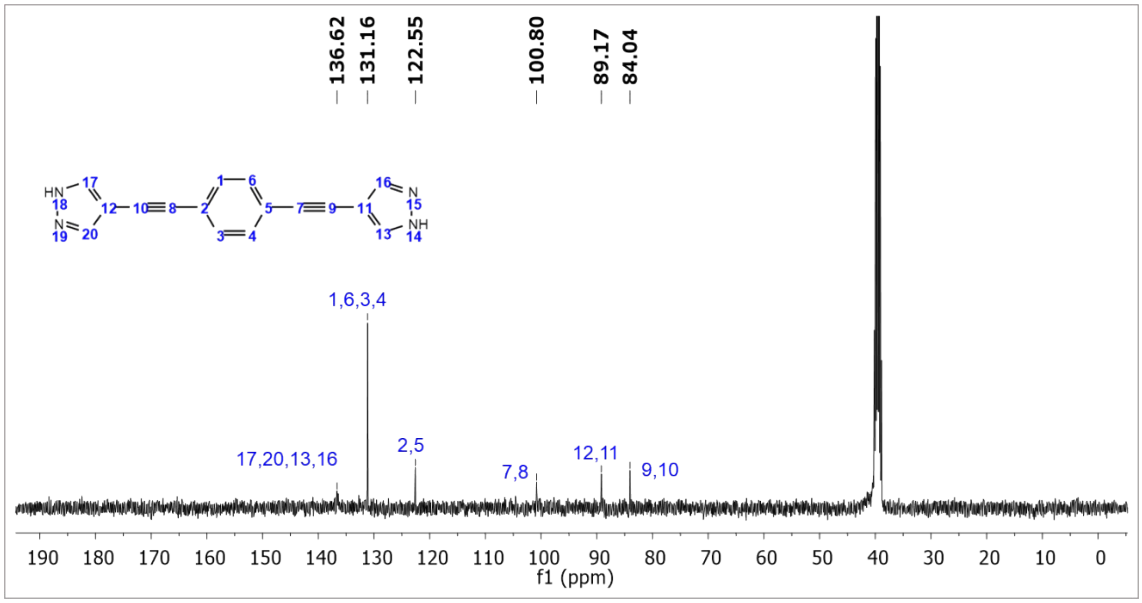

Figure S2. ^{13}C-NMR of compound **1** in DMSO-d6, 100 MHz.

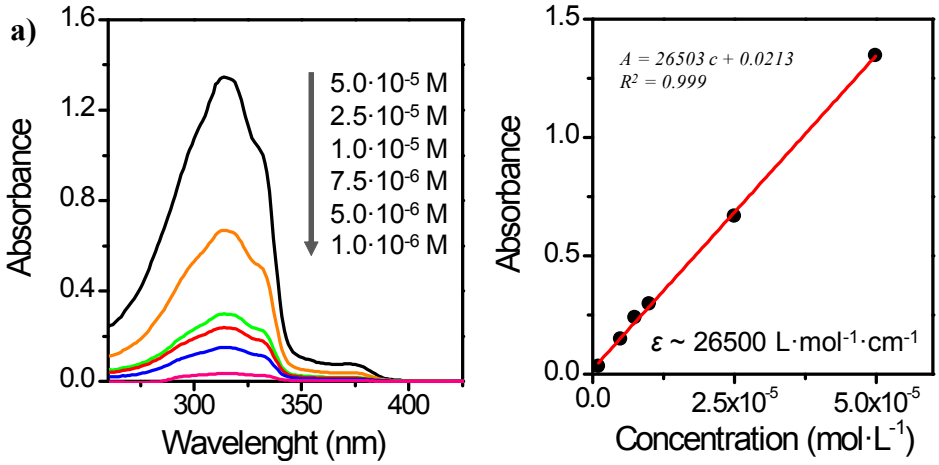

Figure S3. a) UV-Vis spectra registered for compound **1** in THF:$CHCl_3$ (1:4, v/v) at indicated concentrations. **b)** Absorbance vs. concentration lineal fitting (Beer-Lambert law).

2. Deprotonation of the pyrazole group in basic media. ^{1}H-NMR.

Figure S4 displays the ^{1}H-NMR spectrum of **1** in DMSO-d_6 and the spectrum of the same solution after addition of 50 µL of an aqueous NaOH solution (5%). The disappearance of the proton signal associated to the pyrrole-like hydrogen (4.56 ppm) proves that deprotonation of **1** occurs in the basic media. Another observation tentatively associated to this deprotonation process is the change in both the colour of the solution and the light emission of **1**.

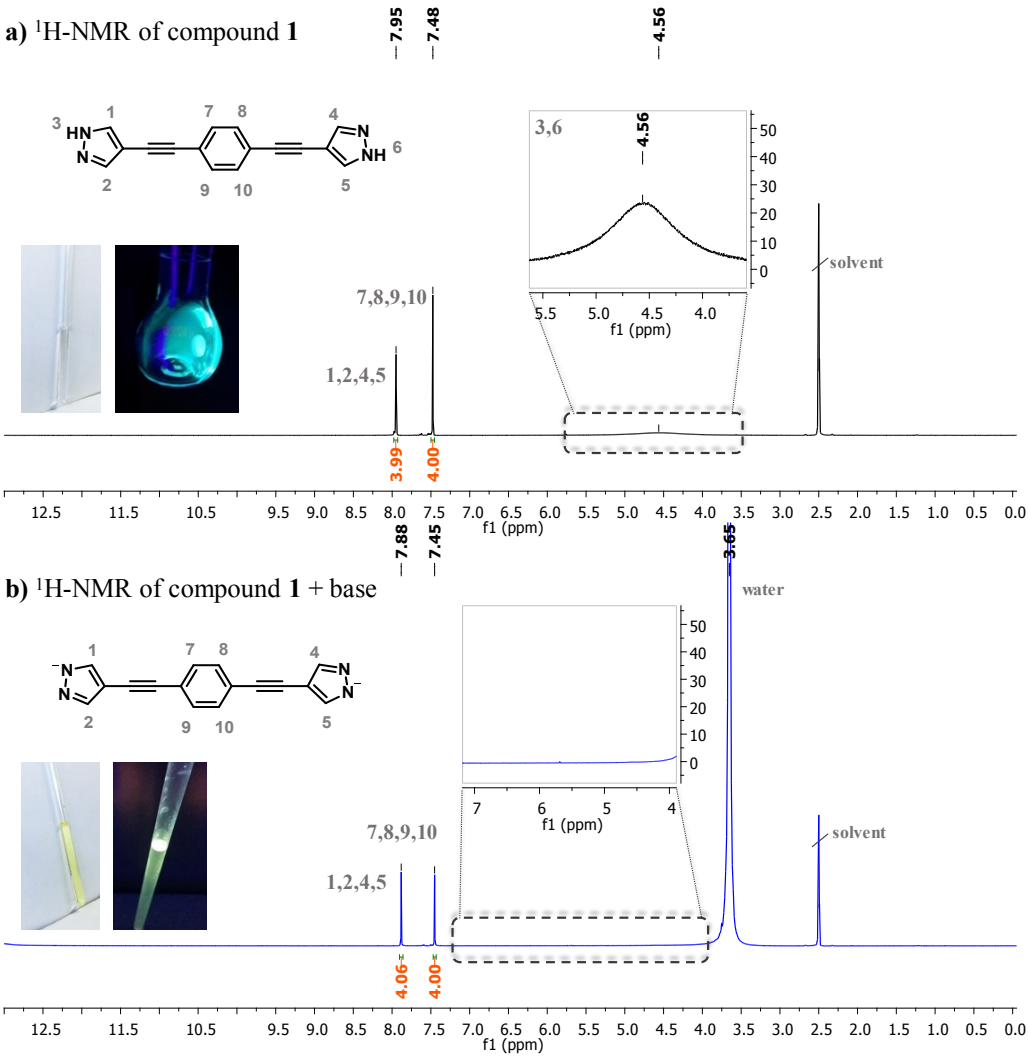

Figure S4. ^{1}H-NMR of **(a)** compound **1** in DMSO-d6 and **(b)** compound **1** in DMSO-d6 after the addition of 50 µL of an aqueous NaOH solution (5%). Zoom in areas 70x. Inset images: white background, pictures taken under natural light; black background, pictures taken under a UV lamp, λ = 365 nm.

3. Extraction of gold atoms from the surface upon gold substrate incubation in a solution of 1.

The self-assembly methodology was used here unsuccessfully to fabricate monomolecular films.

To follow the amount of deposited material with incubation time, a Quartz Crystal Microbalance (QCM from Stanford Research, with circular and both sides patterned gold electrodes, α-quartz crystals (AT-cut) with a resonant frequency of 5 MHz) was used. Clean substrates were immersed in a 10^{-4} M solution of compound **1** in THF:$CHCl_3$ (1:4), the experimental work was repeated twice observing a similar behaviour (Figure S5.a). From the values shown in Figure S5.a, showing a decrease in the amount of deposited

material onto the QCM substrate, it can be generally concluded that **1** is not interacting with the gold QCM substrate in order to form an ordered monolayer. On the contrary, material is lost as the incubation time increases. Supernatant fractions after large incubation times were accumulated on a pre-cleaned cover-glass substrate to be subsequently studied by XPS (one drop from the solution was extracted with a Pasteur pipette and allowed to evaporate onto the cover-glass located in a contaminant protected environment; this procedure was repeated several times).

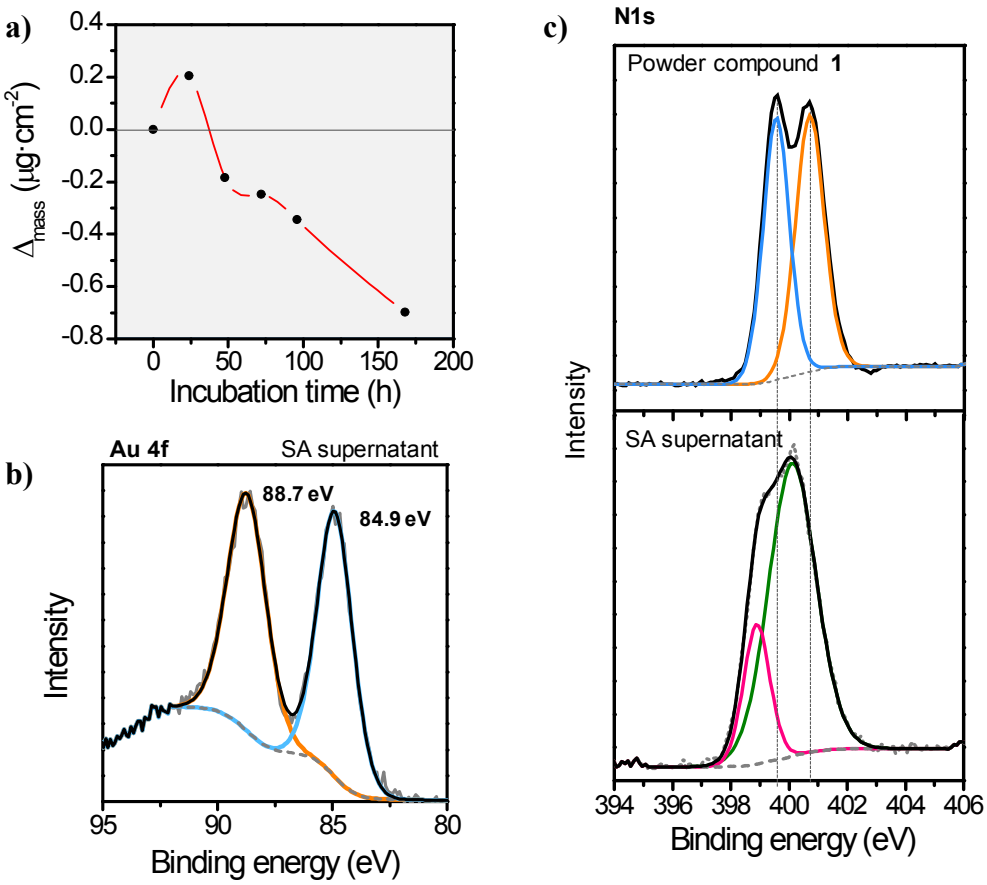

Figure S5. a) Representative QCM experiment showing the mass variation upon incubation time. **b)** XPS spectrum for the high resolution Au4f region registered from the sample prepared by the accumulation/evaporation of several fractions of the supernatant solution. **c)** XPS comparison spectra of the N1s region for: top panel, powder of compound **1**, and bottom panel, the sample holding the accumulation/evaporation of several fractions of the supernatant solution.

The XPS spectrum of the solid residue that results after evaporation of the solvent in the supernatant solution is shown in Figure S5.b (Au4f region). This XPS spectrum reveals the presence of gold (I), with the characteristic $4f_{7/2}$ and $4f_{5/2}$ peaks at 88.7 and 84.9 eV, respectively. Similar binding energies have been previously reported for gold (I) pyrazolate complexes.[1] Additionally, in the N1s region (Figure S5.c. bottom panel) two

peaks can be distinguished at 398.9 eV and 400.2 eV.[2] These binding energies (BE) are different to the BE of the powder compound **1** (399.5 and 400.7 eV) These results are consistent with the formation of gold-pyrazolate complexes[3] where the gold atoms are stripped from the surface of the gold QCM substrate.

4. Surface potential isotherms of Langmuir films of compound 1.

Figure S6 shows the surface potential vs. area per molecule, ΔV-A, isotherms for the monolayer of **1** onto water (pH=5.6) and an aqueous basic of NaOH (pH=11) subphases. ΔV-A isotherms provide complementary information to the π-A isotherms related to the reorientation of molecular dipoles upon the monolayer compression. Additionally, this type of isotherm is more sensitive for the detection of phase transitions than the corresponding π-A isotherm.

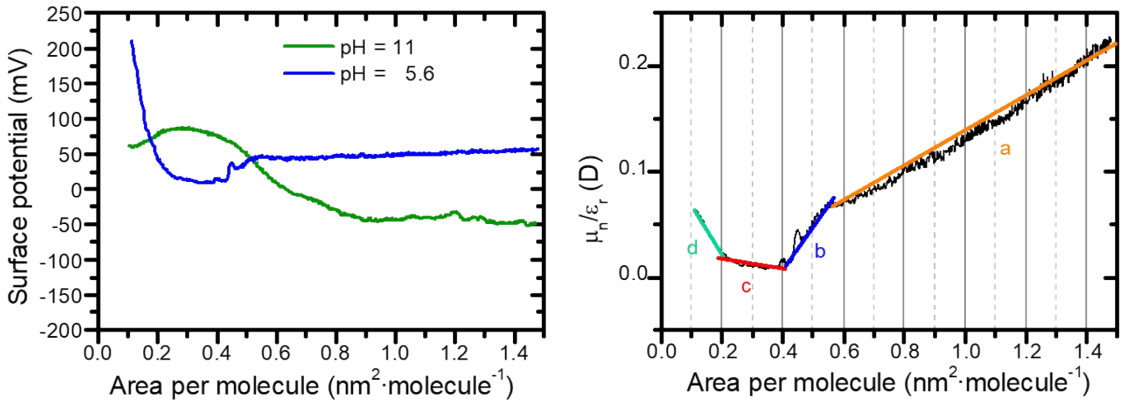

Figure S6. **a)** Surface potential vs. area per molecule isotherms for the monolayer of **1** onto a water subphase (pH = 5.6, blue line) or an aqueous basic subphase (pH = 11, green line); **b)** Apparent normal component of the dipole moment, μ_n / ε_r, for the monolayer of **1** onto water exhibiting four almost linear regions denoted as *a*, *b*, *c* and *d*.

Figure S6.a, shows a different behavior in the surface potential for the monolayer formed onto pure water or onto an aqueous basic subphase. The Langmuir film spread onto pure water shows an initial slightly positive value of surface potential (~ 50 mV), while the film spread onto a basic subphase has an initial negative surface potential (~ -50 mV). The initial different values of the surface potential for the monolayer of **1** prepared onto the basic subphase compared to the isotherm prepared onto water, is attributable to the double layer formed by the ionized pyrazolate headgroups of the monolayer prepared onto a basic subphase.

The surface potential for Langmuir films has been interpreted previously in terms of a model based on the Helmholtz equation.[4] In this model, the monolayer is assumed to behave as a parallel plate capacitor, involving a uniform sheet of evenly distributed dipoles. Following this approach, the value of the surface potential is given by Equation 1:

$$\Delta V = \frac{\mu_n}{A \cdot \varepsilon_r \cdot \varepsilon_0} + \Psi_0 \qquad (1)$$

where the area per molecule is A, the relative dielectric constant and the permittivity of vacuum are ε_r and ε_0, respectively, the normal component of the dipole moment per molecule is μ_n, and in the ionized monolayers Ψ_0 is the double layer contribution. According to the three-layer capacitor model of Demchak and Fort, the surface potential of the monolayer can be expressed as:[5]

$$\Delta V = \frac{1}{A \cdot \varepsilon_0}\left(\frac{\mu_1}{\varepsilon_1} + \frac{\mu_2}{\varepsilon_2} + \frac{\mu_3}{\varepsilon_3}\right) + \Psi_0 \qquad (2)$$

In equation 2, reorientation of water molecules contributes to the term μ_1 / ε_1, while polar and hydrophobic regions of the amphiphilic compound **1** contribute to μ_2 / ε_2 and μ_3 / ε_3, respectively. Local polarizabilities depend on the medium directly enveloping the dipoles, and for this reason different relative dielectric constants, ε_r, are assigned to each of the contributions. Ψ_0 represents the contribution to the surface potential associated to the double-layer potential in ionized monolayers. Since these parameters are difficult to estimate and determine experimentally (ε values are unknown; in addition, they are not constant upon the compression of a monolayer[6]), we do not intend to address here a quantitative study but a qualitative observation of these results.

Figure S6.b shows the μ_n / ε_r values determined from the surface potential isotherm recorded in pure water (assuming $\Psi_0 = 0$ and then $\mu_n / \varepsilon_r = \Delta V \cdot A \cdot \varepsilon_0$), with this plot exhibiting four (approximately) linear regions. The initial value (~ 0.2 Debyes at an area per molecule of 1.5 nm^2) is the larger value obtained for the monolayer of **1**. The almost linear decrease in μ_n / ε_r from 1.5 nm^2 until an area per molecule of 0.56 nm^2. Region *a* in Figure S5.b., is assigned primarily to the reorientation of the water molecules at the interface.[7] The (nearly) linear region in the μ_n / ε_r values (from 0.56 to 0.41 nm^2), denoted as *b* (Figure S5.b) shows a steeper decrease of μ_n / ε_r with decreasing area and is mainly attributed to the reorientation of the pyrazole group, and possibly to the lateral

hydrogen bonds formation between neighbour molecules that results in a decrease of the effective molecule dipole moment. These two regions, namely *a* and *b*, lie within the gas phase of the monolayer. The line with a slightly positive slope denoted as *c* in Figure S6.b. is attributable to the reorientation of the aromatic backbone of the compound and finally, the region denoted as *d* is indicative of the collapse of the monolayer.

5. Topography of the LB films and determination of their thicknesses.

Figures S7.a and S7.b (left panels), show an AFM image of 1x1 μm^2 LB monolayers on a gold on mica substrate. These images are indicative of very homogeneous films free of three-dimensional defects or pores in the structure. Additionally, the thickness of the films was determined using AFM lithography by employing the AFM probe to remove the material and reach the underlying substrate. Then, an area containing both the naked substrate (scratched area) and the monolayer is analysed using Nanoscope V.1.40 software to obtain a statistical value of the monolayer thickness, as shown in Figure S7.a and S7.b (right and middle panels).

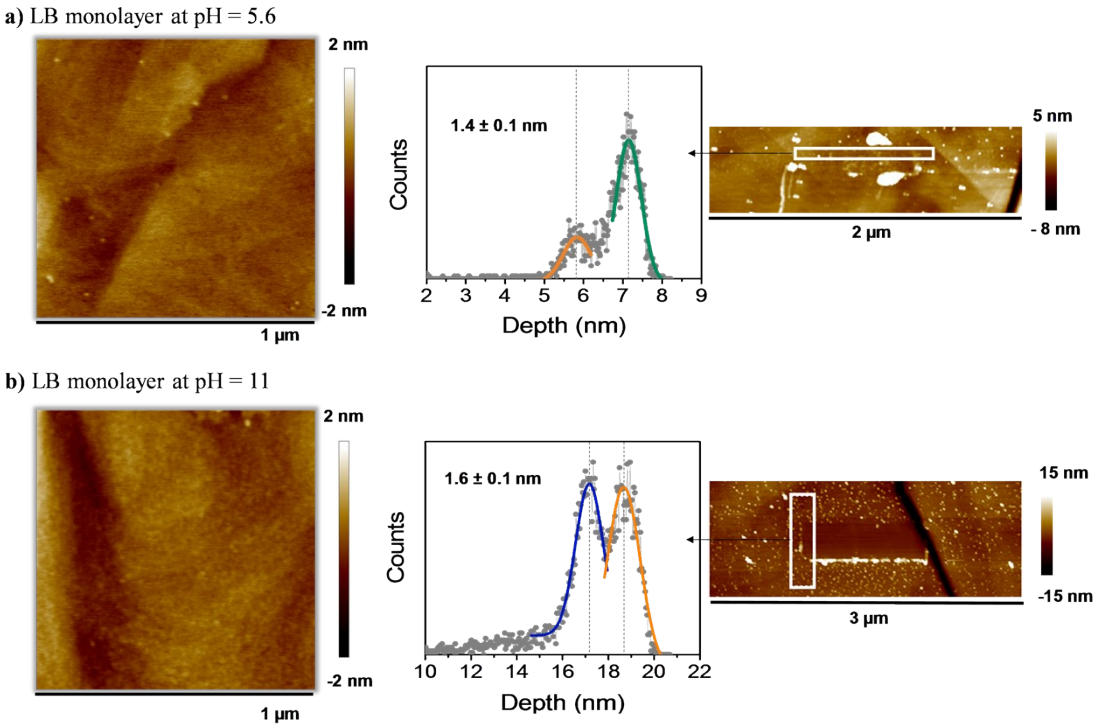

Figure S7. (a) Left: AFM image of a LB monolayer of compound **1** transferred onto a gold on mica substrate at 10 $mN \cdot m^{-1}$ from the air- water interface (pH = 5.6); right and middle panels: scratched area and depth analysis for the determination of the thickness of the monolayer. **(b)** AFM image of a LB monolayer of compound **1** transferred onto a gold on mica substrate at 10 $mN \cdot m^{-1}$ from the air-basic subphase interface (pH = 11.0); right and middle panels: scratched area and depth analysis to determine the film thickness.

6. Conductance measurements. Calibration and *I-V* curves.

In order to appropriately place the STM probe immediately on top of the LB film as required by the TTC method, a prior calibration to determine the initial tip-substrate distance (S_0) has been carried. Details of this distance calibration have been previously reported.[8] Using the following set point parameters I_0 = 10 nA and U_t = 0.6 V, averaged values of $d\ln I/ds$ = 7.2 ± 1.2 nm^{-1} for the LB monolayer fabricated at pH = 5.6 (from 20 $I(s)$ curves) and $d\ln I/ds$ = 5.6 ± 0.8 nm^{-1} for the LB monolayer fabricated at pH = 11.0 (from 20 $I(s)$ curves) were obtained, Figure S8.

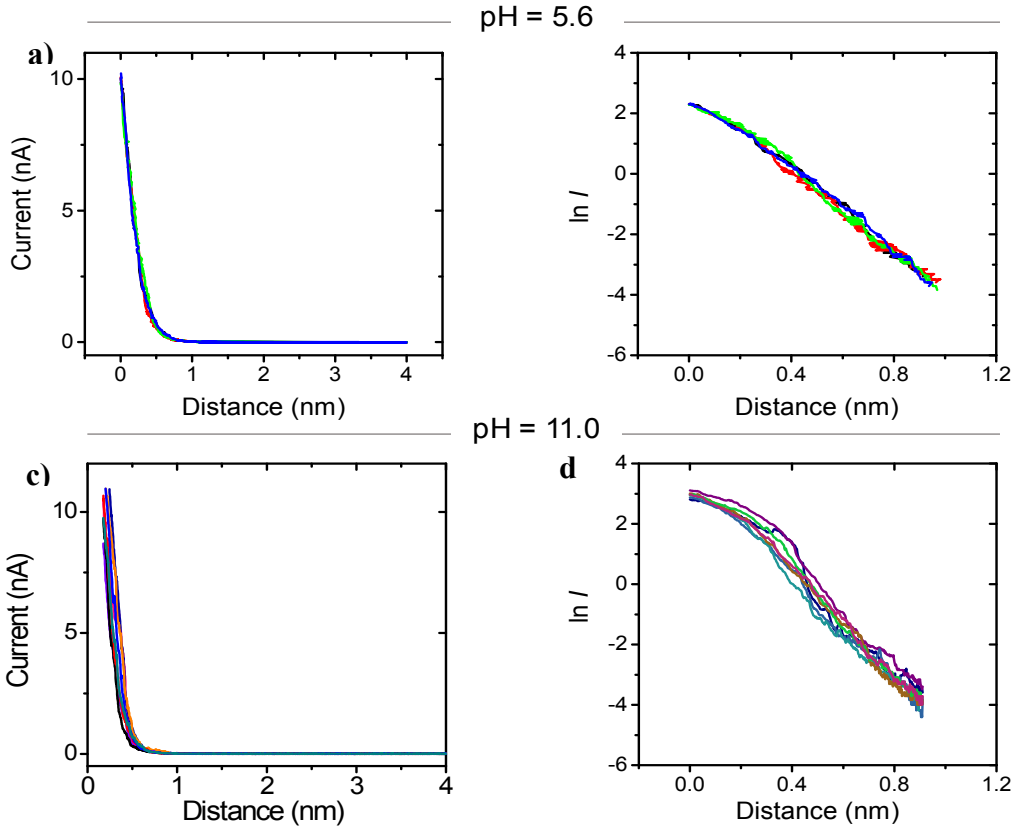

Figure S8. a) and **c)** Examples of $I(s)$ calibration curves registered for the LB monolayer fabricated at the indicated pH values of 5.6 and 11.0. **b)** ln I vs s plots (linear section) deployed for the calibration of the STM probe–substrate distance starting from the $I(s)$ calibration curves at the indicated pH. **d)** ln I vs s plot showing the averaged linear section from 20 $I(s)$ calibration curves (black line) and the linear fitting of the curve in red.

With these determined $d\ln I/ds$ values and keeping the tip bias constant fixed at 0.6 V (U_t = 0.6 V), equation 3 allows one to estimate the set point current (I_o) for which the STM probe would be just contacting the top of the monolayer. In this analysis the

thickness of the LB film used is that determined by AFM lithography, as described above.

$$s_0 = \frac{ln\left(G_0 \cdot U_t/I_0\right)}{dln(I)/ds} \quad (3)$$

where $G_0 = 2e^2/h = 77.5$ μS.

7. References

1. Hendrik, O. L.; Kazushi, K.; Aida, T., Template Sol-Gel Synthesis of Phosphorescent Mesoporous Silica Film Nanocomposites Using an Amphiphilic Gold(I) Pyrazolate Complex. *Adv. Mater. Res.* 2012, **364**, 55-59.
2. Osadchii, D. Y.; Olivos-Suarez, A. I.; Bavykina, A. V.; Gascon, J., Revisiting Nitrogen Species in Covalent Triazine Frameworks. *Langmuir* 2017, **33**, 14278-14285.
3. Barberá, J.; Elduque, A.; Giménez, R.; Oro, L. A.; Serrano, J. L., Pyrazolate"Golden" Rings: Trinuclear Complexes That Form Columnar Mesophases at Room Temperature. *Angew. Chemie Int. Ed. English* 1996, **35**, 2832-2835.
4. Helmholtz, H., *Abhandlungen Thermod.* 1902, **51**.
5. Demchak, R. J.; Fort, T., Surface dipone-moments of close-packed un-ionized monolayers at air-water interface. *J. Colloid and Interf. Science* 1974, **46** (2), 191-202.
6. Oliveira Jr., O. N.; Taylor, D. M.; Morgan, H., *Thin Solid Films* 1992, **210/211**, 76.
7. Tsukanova, V.; Salesse, C., On the Nature of Conformational Transition in Poly(ethylene glycol) Chains Grafted onto Phospholipid Monolayers. *J. Phys. Chem. B* 2004, **108** (30), 10754-10764.
8. Pera, G.; Martin, S.; Ballesteros, L. M.; Hope, A. J.; Low, P. J.; Nichols, R. J.; Cea, P., Metal-Molecule-Metal Junctions in Langmuir-Blodgett Films Using a New Linker: Trimethylsilane. *Chem. Eur. J.* 2010, **16** (45), 13398-13405.